Antimatter transport processes

D P van der Werf[1]**, G B Andresen**[2]**, M D Ashkezari**[3]**,
M Baquero-Ruiz**[4]**, W Bertsche**[1]**, P D Bowe**[2]**, C C Bray**[4]**, E Butler**[1]**,
C L Cesar**[5]**, S Chapman**[4]**, M Charlton**[1]**, J Fajans**[4]**, T Friesen**[6]**,
M C Fujiwara**[6,7]**, D R Gill**[6]**, J S Hangst**[2]**, W N Hardy**[8]**, R S Hayano**[9]**,
M E Hayden**[3]**, A J Humphries**[1]**, R Hydomako**[6]**, S Jonsell**[1,10]**,
L V Jørgensen**[1]**, L Kurchaninov**[7]**, R Lambo**[5]**, N Madsen**[1]**,
S Menary**[11]**, P Nolan**[12]**, K Olchanski**[7]**, A Olin**[7]**, A Povilus**[4]**, P Pusa**[11]**,
F Robicheaux**[13]**, E Sarid**[14]**, D M Silveira**[9,15]**, C So**[4]**, J W Storey**[7]**,
R I Thompson**[6]**, J S Wurtele**[4]** and Y Yamazaki**[15]
(ALPHA Collaboration)

[1] Department of Physics, Swansea University, Swansea SA2 8PP, United Kingdom
[2] Department of Physics and Astronomy, Aarhus University, DK-8000 Aarhus C, Denmark
[3] Department of Physics, Simon Fraser University, Burnaby BC, V5A 1S6, Canada
[4] Department of Physics, University of California, Berkeley, CA 94720-7300, USA
[5] Instituto de Física, Universidade Federal do Rio de Janeiro, Rio de Janeiro 21941-972, Brazil
[6] Department of Physics and Astronomy, University of Calgary, Calgary AB, T2N 1N4, Canada
[7] TRIUMF, 4004 Wesbrook Mall, Vancouver BC, V6T 2A3, Canada
[8] Department of Physics and Astronomy, University of British Columbia, Vancouver BC, V6T 1Z4, Canada
[9] Department of Physics, University of Tokyo, Tokyo 113-0033, Japan
[10] Fysikum, Stockholm University, SE-10691, Stockholm, Sweden
[11] Department of Physics and Astronomy, York University, Toronto, ON, M3J 1P3, Canada
[12] Department of Physics, University of Liverpool, Liverpool L69 7ZE, United Kingdom
[13] Department of Physics, Auburn University, Auburn, AL 36849-5311, USA
[14] Department of Physics, NRCN-Nuclear Research Center Negev, Beer Sheva, IL-84190, Israel
[15] Atomic Physics Laboratory, RIKEN, Saitama 351-0198, Japan

E-mail: D.P.van.der.Werf@Swansea.ac.uk

Abstract. A comparison of the 1S-2S transitions of hydrogen and antihydrogen will yield a stringent test of CPT conservation. Necessarily, the antihydrogen atoms need to be trapped to perform high precision spectroscopy measurements. Therefore, an approximately 0.75 T deep neutral atom trap, equivalent to about 0.5 K for ground state (anti)hydrogen atoms, has been superimposed on a Penning-Malmberg trap in which the anti-atoms are formed. The antihydrogen atoms are produced following a number of steps. A bunch of antiprotons from the CERN Antiproton Decelerator is caught in a Penning-Malmberg trap and subsequently sympathetically cooled and then compressed using rotating wall electric fields. A positron plasma, formed in a separate accumulator, is transported to the main system and also compressed. Antihydrogen atoms are then formed by mixing the antiprotons and positrons. The velocity of the anti-atoms, and their binding energies, will strongly depend on the initial conditions of the constituent particles, for example their temperatures and densities, and on the details of the mixing process. In this paper the complete lifecycle of antihydrogen atoms will be presented, starting with the production of the constituent antiparticles and the description of the manipulations necessary to prepare them appropriately for antihydrogen formation. The latter will also be described, as will the possible fates of the anti-atoms.

1. Introduction

It has become routine in recent years to produce antihydrogen at low energies via the controlled mixing of antiproton and positron clouds. Currently, much of the effort is devoted to attempts to trap antihydrogen in a magnetic minimum neutral atom trap in preparation for spectroscopic interrogation of its states and comparisons with hydrogen; (see e.g. [1, 2]). Complex apparatus [3, 4, 5], involving traps for the charged particles with superimposed atom traps, have been assembled for this purpose and are presently in development and operation.

In order to promote antihydrogen capture in the state-of-the-art, sub-K deep, neutral traps available to us, the positrons and antiprotons have to be collected and carefully manipulated before they are mixed together to promote combination. Many of the techniques that have been developed to achieve this involve transport of the antiparticles. Typically this will include collisions with buffer gas and/or interactions with clouds of electrons, often in the presence of time-varying electric fields designed to manipulate the radial profile of the charged plasmas. Transport is also a feature of the antihydrogen formation process itself, since the repeated formation and break-up of loosely bound anti-atoms can result in the antiprotons being transported to the outskirts of the positron cloud, or beyond [6, 7].

This article will contain a brief introduction to the techniques involved in antiparticle manipulation for antihydrogen formation with particular emphasis on aspects involving charged particle transport. A recent summary of positron transport phenomena in gases can be found in [8].

2. Traps and Plasmas

Most of the processes and techniques described in this paper take place in Penning traps, which are a common workhorse for charged particle confinement. This is achieved by arranging a series of (typically) cylindrical electrodes along the axis of a solenoid. The combination of the magnetic field of magnitude B (which provides the radial confinement for the particles) and the electric fields due to the voltages applied to the electrodes, results in three-dimensional confinement. The motion of a single particle, or a small collection of them, in such a trap is well understood (see e.g. [9]). Simplifying somewhat, a particle of mass, m, and charge, q, will undergo an axial (conventionally the z-direction) bounce motion with an angular frequency $\omega_z = \sqrt{2qV_0/(md^2)}$, where V_0 and d are characteristic trap voltages and dimensions, respectively. The radial component is composed of two superimposed motions: the familiar cyclotron motion with an angular frequency $\omega_c = qB/m$ and a slower magnetron drift of frequency $\omega_m = \omega_z^2/(2\omega_c) = V_0/(Bd^2)$.

It is commonplace, however, that the antiparticle clouds are sufficiently dense that they form so-called single-component plasmas. Here the Debye screening length, $\lambda_D = \sqrt{k_B T \epsilon_0/(n_e q^2)}$ (where n_e and T are the density and temperature of the cloud, respectively) is smaller than all the physical dimensions of the cloud. Note that λ_D is the length over which external electric fields are shielded by particles at the edge of the plasma. Collective plasma oscillations can be important (see e.g [10]) and can even be used as plasma diagnostics [11, 12].

Of particular note is the self electric field of the plasma, which is radial in nature with, for spheroidal plasmas, a magnitude $E_r = n_e qr/(2\epsilon_0)$. This field effectively replaces the shielded trap electric field and modifies the magnetron, or $\mathbf{E} \times \mathbf{B}$, drift which now has a characteristic angular frequency [10] $\omega_D = E_r/B = n_e q/(2\epsilon_0 B)$. Note that this implies that an antiproton at a radial distance r will have a transverse speed associated with this motion of $v_r = \omega_D r$, which will contribute to the kinetic energy of the atom if the antiproton forms antihydrogen. It is easy to see, for the parameters common in antihydrogen experiments (see e.g. [7]), that this kinetic energy can exceed that due to the thermal energy of the plasmas. This "drift" kinetic energy is proportional to r^2 and can be reduced by working with clouds of small radii. This is one of the main motivating factors behind the manipulation and transport schemes developed

for antihydrogen experimentation, which we now outline.
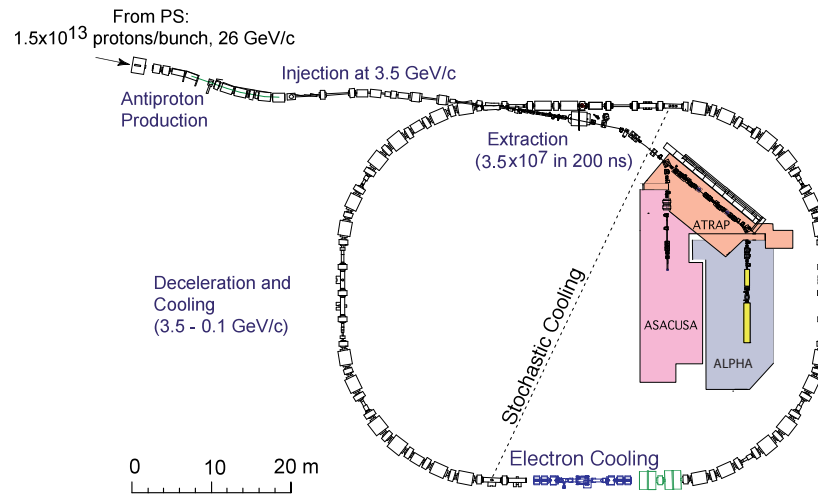
Figure 1. Schematic illustration of the AD ring.

3. Antiproton Capture, Cooling and Compression

The Antiproton Decelerator (AD) facility at CERN [13] is presently the only place in the world producing relatively low energy antiprotons. Figure 1 shows a schematic of the AD ring and the positions of the experiments. Every 100 seconds, protons with a momentum of 26 GeV/c hit a fixed target, producing antiprotons via $p + p \rightarrow p + p + p + \overline{p}$. A bunch of about 10^7 $\overline{p}$'s approximately 200 ns long, emanating from the target at around 3.5 GeV/c, is captured in the AD ring. To prevent the bunch from blowing up during deceleration, the antiparticles are cooled in four stages using stochastic [13] and electron [14] cooling techniques.

The antiprotons entering the ALPHA apparatus are still far too energetic for antihydrogen formation. Thus, a thin foil is mounted at the entrance of the ALPHA trap (degrader in figure 2a) and a small fraction of the antiprotons are slowed down to trappable energies and enter the electrode stack, which has a 4 kV potential applied at one end (figure 2b). The antiprotons bounce back and before they are able to leave the trap a 4 kV potential is raised on an electrode near the degrader, thereby confining the antiparticles (figure 2c).

Although now trapped, there is no mechanism for the antiprotons to cool down. Therefore, to enable cooling, a cloud of electrons is injected in the trap before the antiprotons arrive. The electrons cool down by synchrotron cooling in about 0.4 s when immersed in a magnetic field of 3 T and in turn they cool the antiprotons via the Coulomb interactions in about 20 s. Note that the synchrotron cooling rate is proportional to m^{-3} so that it would take of the order of a century for the antiprotons to cool down via this process.

When trapped and cooled, the antiproton cloud does not yet have the optimum shape (radius, length) and/or density for antihydrogen experimentation. However, it is possible to compress plasmas by applying a rotating electric dipole or quadrupole field [15]; the so-called rotating wall technique. This can be implemented by azimuthally segmenting one of the confining electrodes and applying a sinusoidal voltage to the segments, with each having a different phase with respect to the others.

The antiprotons were compressed by applying the rotating wall technique on the electron plasma containing the antiprotons [16] for a certain time. The radial profile of both the electrons and antiprotons were subsequently determined by ejecting the particles onto a MCP/Phosphor screen assembly residing outside the main ALPHA system (see figure 4a) [17]. Figure 3 shows
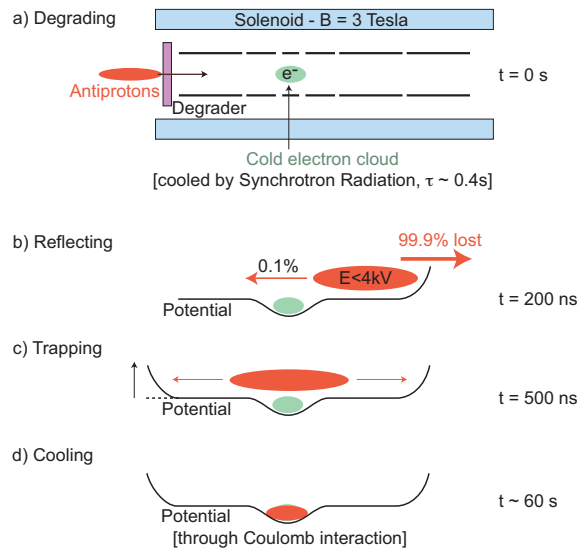
Figure 2. (a) Antiprotons arrive from the AD (to the left) with 5.3 MeV kinetic energy and are decelerated in the degrader, which is a metal foil of about 0.1 mm thickness. Electrons have been loaded previously into a centrally located trap. (b) An electrostatic wall, formed by an electrode held at high voltage is erected before the antiprotons arrive. Antiprotons with low enough energy are reflected back towards the degrader. (c) About 500 ns after the antiprotons arrive the entrance is closed by erecting a similar wall, and the antiprotons are trapped. (d) About 60 s later the antiprotons have cooled down through collisions with the cold (and self-cooling) electrons.
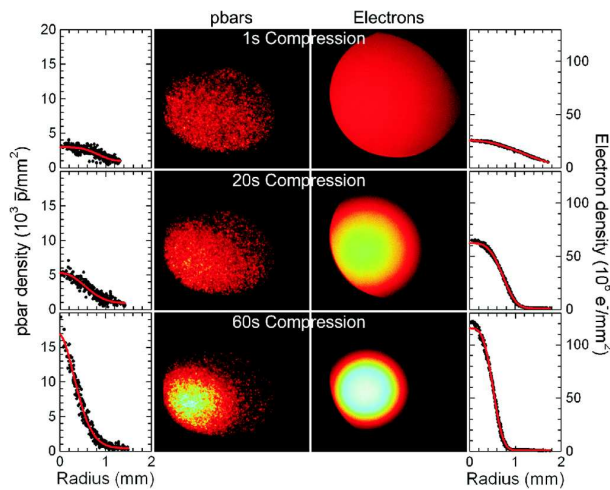
Figure 3. Antiproton and positron images showing the effects of compression, and the resulting radial profiles. The solid (red) lines are Gaussian-like (i.e., $\exp(-[r/r_0]^k)$, where $k \approx 2$) fits to the radial profiles.

examples of the phosphor screen image after applying the rotating wall for 1, 20 and 60 seconds. The antiproton images are shown on the left side, with the outer left column displaying the radial profile. The right side shows the corresponding electron data. It can be observed that the radial extent of both species reduces as the rotating wall is applied for longer durations.

Both the formation rate and the trapping probability of antihydrogen are dependent on the
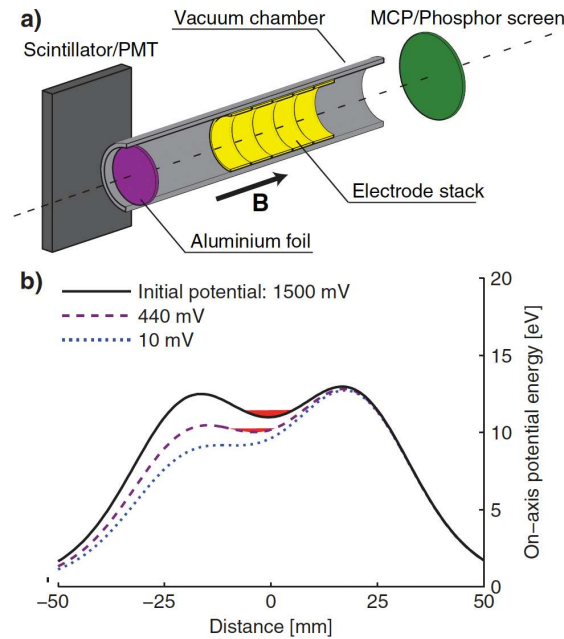
Figure 4. (a) Simplified schematic of the Penning-Malmberg trap used to confine the antiprotons and of the two diagnostic devices used. The direction of the magnetic field is indicated by the arrow. (b) Potential wells used to confine the antiprotons during the evaporative cooling ramp. The antiprotons are indicated at the bottom of the potential well (red), and the different wells are labelled by their on-axis depth.

temperature of the constituent particles. Therefore, ALPHA applied the evaporative cooling technique, well known for its use on atoms, for the first time to a cryogenic, non-neutral plasma, in this case consisting of antiprotons [18]. The temperature of the cloud was determined by lowering the potential on one side, thus allowing antiprotons to leave and hit an aluminium foil (see figure 4a) where they annihilated. The annihilation products were detected using the external scintillator/PMT arrangement. If the particles are in thermal equilibrium, the energy distribution of the first particles to escape, found from mapping the arrival time at the foil to the well depth, will follow the Boltzmann distribution [19].

For each experiment 45,000 antiprotons were prepared in a plasma with a radius of 0.6 mm and density of 7.5×10^6 cm^{-3}. Subsequently, the potentials were linearly lowered to a well with a certain depth (a few examples are shown in 4b) and the temperature was measured using the method above. In figure 5, six measurements are shown and the lowest temperature achieved was (9 ± 4) K using a 10 mV deep well, when (6 ± 1) % of the antiprotons remained trapped.

4. Positron Accumulation, Compression, Transfer and Cooling

Positrons are accumulated using a 3-stage Surko-type buffer gas device (see figure 6) [20]. Positrons emanating from a 2 GBq ($\approx$ 75 mCi) ^{22}Na source are slowed using a solid neon moderator [21, 22]. The neon is condensed directly onto the source which is mounted on a cold finger connected to a closed cycle helium refrigerator capable of reaching temperatures down to 4 K. The moderated positrons are then accelerated to 80 eV and transported into the first stage of the electrode stack. Nitrogen gas is admitted into this stage at a pressure of about 10^{-3} mbar, and, due to the increased diameters of following stages, pressures of 10^{-4} and 10^{-6} mbar are established in, respectively, the second and third stages. The relatively high pressure in the first stage causes the positrons to lose enough kinetic energy in an inelastic collision with the
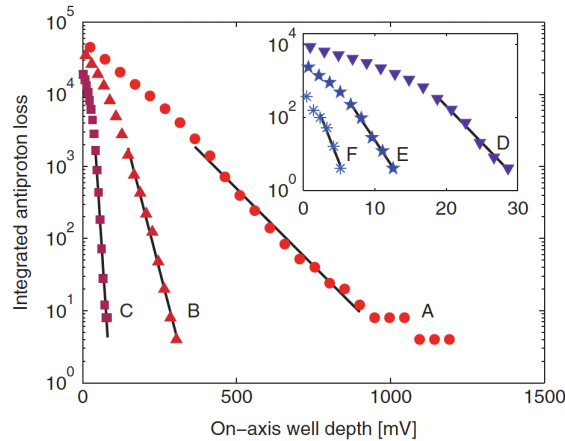
Figure 5. The number of antiprotons lost from the well as its depth is reduced is integrated over time and plotted against the well depth. The well depth was ramped from high to low; thus, time flows from right to left in the figure. The measured number was corrected for the 25 % detection efficiency. The curves are labelled in decreasing order of the temperatures extracted from an exponential fit, shown as the solid lines. The temperatures extracted are: A: 1040, B: 325, C: 57, D: 23, E: 19, and F: 9 K. As the antiprotons get colder, fewer can be used to determine their temperature, an effect described in Ref. [19].
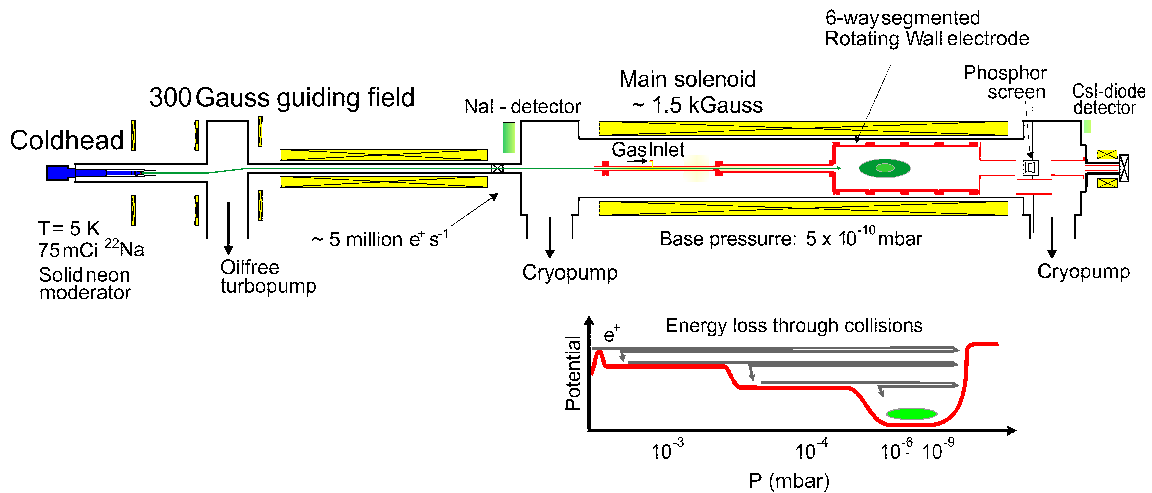
Figure 6. Schematic illustration of the positron beamline and buffer gas accumulator. The lower panel is a representation of the axial electrical potential of the trap and shows how collisions, progressively in each stage, result in accumulation in the third stage. When the nitrogen line is closed, the gas is pumped out promptly [20] in readiness for transfer of the positrons to the main ALPHA system.

gas before they can escape the trap. As shown on the lower panel of figure 6, further collisions in stages two and three results in positron accumulation in the latter. The low pressure in stage three reduces the annihilation probability and the rate of radial transport of the trapped positrons such that lifetimes of around 100 s can be achieved routinely.

It is advantageous to reduce as far as possible the radial extent of the accumulated positrons since, on transfer, they must pass through a small pumping restriction which separates the main

(a)   (b)   (c)
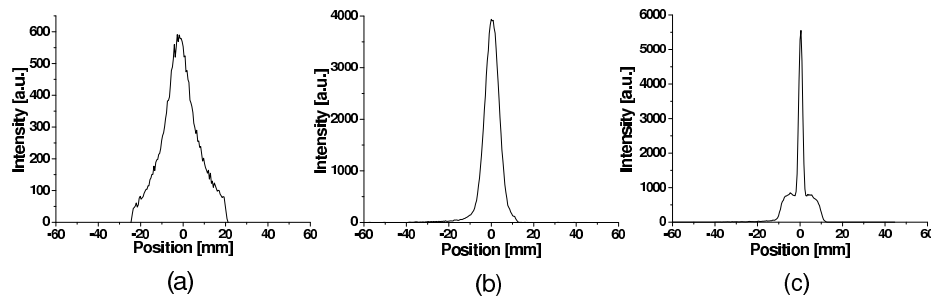
Figure 7. One dimensional projection of the phosphor screen image of the ejected positron cloud following dipolar rotating wall compression. (Note that the overall distribution is ellipsoidal.) (a) no rotating wall; (b) rotating wall with N_2 gas only and (c) rotating wall with N_2 and added CO_2 cooling gas. The integrated yields are around 29, 38 and 30 million positrons for (a), (b) and (c) respectively.

ALPHA system from the accumulator. Thus, a rotating wall is employed in the accumulator to compress the positrons and figure 7 shows radial profiles measured using the phosphor screen (figure 6) with and without the rotating wall. Using the rotating wall during accumulation at a fixed frequency of 700 kHz narrows the radial profile (figure 7b), and plasmas sizes of 7 mm diameter have been obtained. Interestingly, inserting a cooling gas such as CO_2 [23], the radial profile can be changed dramatically as shown in figure 7c. More research is needed to understand these data, which seem to indicate that there are two radial distributions within the accumulator.
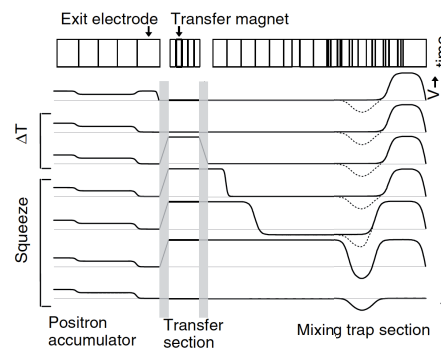

Figure 8. Schematic of the electrode system used to transfer and re-trap the positrons. The time sequence of the potentials is shown. A pulsed magnetic field of around 1 T for 1 s was applied using the so-called transfer magnet to squeeze the positrons through a narrow pumping restriction.

After accumulation and subjecting the positrons to the desired rotating wall manipulation, the nitrogen buffer gas is pumped out and the positrons are transported into the main ALPHA system [24]. Figure 8 illustrates how the potential changes in time during the transport procedure. The upper three lines show the potential of the accumulator exit electrode dropping rapidly to allow the positrons to escape and then the first electrode in the main system closing after a time ΔT to re-trap them. The well size was then slowly squeezed until the positrons cooled (in the 1 T magnetic field) into a small well in the mixing section. Once held there, the process could be repeated and stacking of positrons achieved [24]. In the cryogenic environment of the

ALPHA system, the positron lifetime is extremely long (and is more-or-less immeasureable), such that long timescale operations extending over many hours can be undertaken if required. Dedicated experiments by the ATHENA collaboration [24, 25], working under similar conditions to those of ALPHA, stacked 40 positron plasmas containing, in total, around 1.2×10^9 particles and with overall densities up to $2.6 \times 10^{10} \mathrm{cm}^{-3}$.

5. Antihydrogen Formation

Once the antiprotons and positrons are held together in the ALPHA mixing region (see figure 9) they are merged to form antihydrogen. In ATHENA, this was achieved by injecting the antiprotons into the positrons with several eV of kinetic energy [26]. It was found, however, that this produced antihydrogen before the antiprotons had fully slowed in the positrons, [27]; i.e. with kinetic energies above thermal, and which would preclude trapping. Accordingly, ALPHA has developed new mixing methodologies, which will be described elsewhere [28], to allow the antiprotons to enter the positron plasma with minimal addition to their kinetic energy.
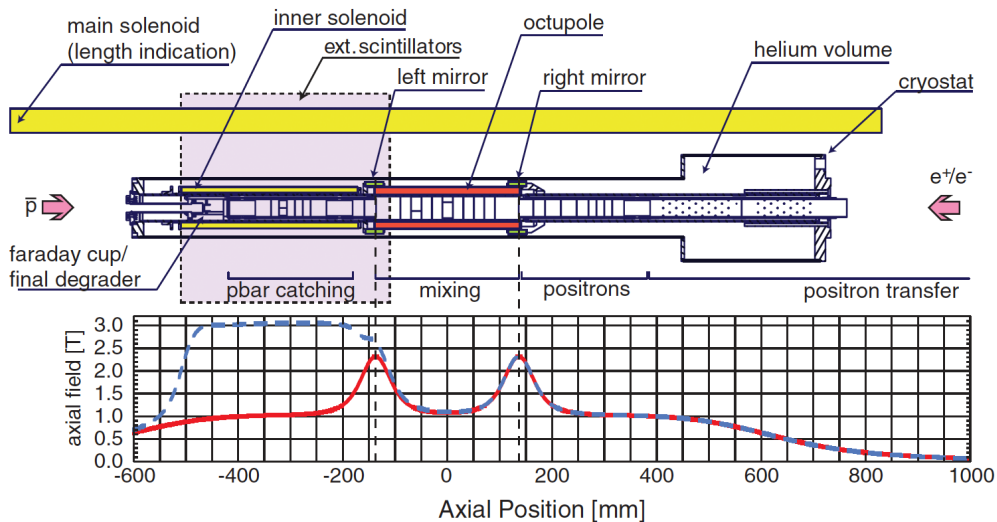
Figure 9. Schematic diagram of the ALPHA apparatus. The graph shows the on-axis longitudinal magnetic field due to the solenoids and mirror coils. The blue (red) curve is the field with (without) the inner solenoid. The positron accumulator (not pictured) is located to the right of the apparatus. The positrons and antiprotons are held and manipulated in the marked regions before transfer to the mixing section, where further manipulations, including evaporative cooling, are performed.

At the positron temperatures and densities used in most antihydrogen experiments to date it is expected that the three-body formation reaction (TBR), $e^+ + e^+ + \overline{p} \rightarrow \overline{H} + e^+$, will dominate over the spontaneous radiation recombination process, $e^+ + \overline{p} \rightarrow \overline{H} + h\nu$. This is supported by some direct evidence, such as the rate of antihydrogen production, which is many times that expected from the radiative reaction [18, 29] and the abundant production of weakly bound states [18, 30], which is a characteristic of the TBR.

The TBR has textbook dependencies on T and n_e and as $n_e^2 T^{-9/2}$, and is expected to occur with a rate of $\approx 4 \times 10^{-9} n_e^2 T^{-9/2}$ s^{-1} (with n_e in units of cm^{-3} and T in K), which applies in thermodynamic equilibrium, with zero external fields and for plasmas of essentially infinite extent, such that none of the species can reach a boundary. However, the manner in which antiprotons and positrons are mixed in antihydrogen experiments is far from this ideal.

Following simulation work by Robicheaux and co-workers [31, 32] it has become apparent that the conditions which apply in the antihydrogen experiments, and in particular the finite size of the positron plasmas, have a profound influence on the distributions of binding energy and speed of the antihydrogen, as well as on the fate of the antiprotons. This has been highlighted by recent detailed simulations of the ATHENA experiment [6].

A particular finding, also mentioned by Robicheaux [31], is that it is misleading to consider the straightforward TBR as a "one-way street" to antihydrogen formation. Indeed, weakly bound antihydrogen is formed readily in the positron plasma, but in most cases is ionized in further collisions with the positrons. This can proceed very rapidly since the cross sections for collisions of such Rydberg-like species can be very high ($> 10^{-13}$ cm^2). Thus, it may be more appropriate to write a three-body scenario as follows:

$$e^+ + e^+ + \overline{p} \rightarrow \overline{H}^{**} + e^+ \rightarrow \overline{H}^* + e^+$$
$$\text{or} \tag{1}$$
$$\rightarrow e^+ + e^+ + \overline{p},$$
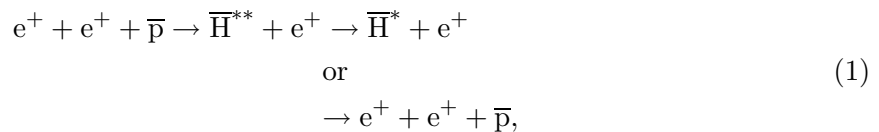
where the asterisks denote degrees of internal excitation. The branching ratio of the two outcomes is overwhelmingly in favour of re-ionization such that the antiproton is recycled. Here we denote $\overline{H}^*$ as an excited antihydrogen atom which is produced from a higher state in collision. Notwithstanding, in order for the antihydrogen to be detected via its annihilation on the electrode walls of the Penning trap, it must survive the trap fields and the electric field of the plasma. Recall from section 2 that the latter has a radial dependence as $E_r \propto r$ such that the field will be highest at the plasma outer edge. (The detailed mechanism of field ionization by the radial field in the plasma has been elucidated in [6].) The effects of antihydrogen atoms field ionized at large radial distances (outside the positron plasma) were also recently observed by the ALPHA experiment [18]. In this case the remnant antiprotons were swept to the electrode walls due to the presence of an octupolar magnetic field used to promote anti-atom trapping.

The repeated formation and ionization of antihydrogen via the reaction schema (1) has a marked effect on the radial distribution of the antiprotons. When they are neutralised as antihydrogen the antiprotons are no longer tightly pinned by the magnetic field and the nett effect is that they are transported across the field lines and can quickly reach the edge of the plasma. Thus, antiprotons can reside in a shell on the outskirts of the plasma where they might eventually form antihydrogen but which will gain extra kinetic energy from the radial drift which, for many combinations of n_e and r, will make trapping impossible. Therefore, it is important to understand and control this mechanism of antihydrogen formation-mediated antiproton transport in order that the fraction of antiprotons that form trappable antihydrogen can be maximized. The effect is illustrated by the results of the simulations [6] as shown in figure 10. Here the yield of antihydrogen, both detected via annihilation and field ionized, is plotted versus the difference, Δr, between the formation position of antihydrogen and the position at which it leaves the positron plasma, for two different values of n_e. Note the logarithmic scale, the marked differences between the distributions at the two densities and the very large fraction of ionized antihydrogen at small Δr. It is these antihydrogen atoms which result in the antiprotons residing on the edge of the positron plasma due to the aforementioned transport. Much experimental effort has been expended to control the effects of this by manipulating the radial profiles and the densities of the plasmas prior to mixing; added insights from transport theories and simulations would be welcome.

6. Conclusion

We have given a brief overview of aspects of antihydrogen formation, most particularly for the ALPHA experiment which aims to trap antihydrogen in a magnetic minimum neutral atom trap
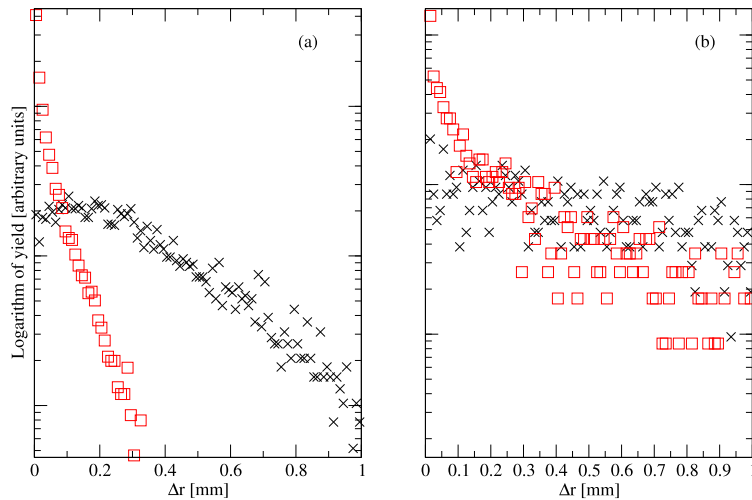
Figure 10. The distribution of the difference in radius between the point of formation of antihydrogen atoms and the point at which they left the positron plasma, for ($\times$) detected and ($\square$) ionized antihydrogen, (a) $n_e = 10^9$ cm^{-3}, (b) $n_e = 5 \times 10^7$ cm^{-3}.

to promote spectroscopic comparisons of the anti-atom with hydrogen. Many of the techniques that have been developed to achieve this involve transport phenomena, and we have highlighted a few examples. Further effort is required to develop antihydrogen into a tool to probe new physics, and much is based upon our understanding and manipulation of the underlying reaction dynamics; theoretical input has always been an important element of this emerging field [33], and there would be great added value from an enhanced understanding of antimatter transport physics.

7. Acknowledgements

8. References

[1] Charlton M, Jonsell S, Jørgensen L V, Madsen N and van der Werf D P 2008 *Cont. Phys.* **49** 29
[2] Madsen N 2010 *Proc. Roy. Soc.* **368** 3671
[3] Bertsche W *et al* (ALPHA collaboration) 2006 *Nuc. Inst. Meth. in Phys. Res. A* **566** 746
[4] Andresen G B *et al* (ALPHA collaboration) 2007 *Phys. Rev. Lett.* **98** 023402
[5] Gabrielse G *et al* (ATRAP collaboration) 2008 *Phys. Rev. Lett.* **100** 113001
[6] Jonsell S, van der Werf D P, Charlton M and Robicheaux F 2009 *J. Phys. B: At. Mol. Opt. Phys.* **42** 215002
[7] Andresen G B *et al* (ALPHA collaboration) 2010 *Phys. Lett. B* **685** 141
[8] Charlton M 2009 *J. Phys. Conf. Series* **162** 012003
[9] Major F G, Gheorghe V N and Werth G 2005 *Charged Particle Traps: Physics and Techniques of Charged Particle Field Confinement* (Springer, Berlin)
[10] Davidson R C 1990 *An Introduction to the Physics of Nonneutral Plasmas* (Addison-Wesley)
[11] Amoretti M *et al* (ATHENA collaboration) 2003 *Phys. Rev. Lett.* **91** 055001

[12] Amoretti M *et al* (ATHENA collaboration) 2003 *Phys. Plasmas* **10** 3056
[13] Maury S 1997 *Hyperfine Interact.* **109** 43
[14] Budker G I and Skrinskii A N 1978 *Sov. Phys. Usp.* **21** 277
[15] Anderegg F, Hollman E M and Driscoll C F 1998 *Phys. Rev. Lett.* **81** 4875
[16] Andresen G B *et al* (ALPHA collaboration) 2008 *Phys. Rev. Lett.* **100** 203401
[17] Andresen G B *et al* (ALPHA collaboration) 2009 *Rev. Sci. Inst.* **80** 123701
[18] Andresen G B *et al* (ALPHA collaboration) 2010 *Phys. Rev. Lett.* **105** 013003
[19] Eggleston D L, Driscoll C F, Beck B R and Hyat A W 1992 *Phys. Fluids B* **4** 3432
[20] Surko C M, Greaves R G and Charlton M 1997 *Hyperfine Interact.* **109** 181
[21] Mills Jr A P, and Gullikson E M 1986 *Appl. Phys.* **49** 1121
[22] Khatri R, Charlton M, Sferlazzo P, Lynn K G, Mills Jr A P and Roellig L O 1990 *Appl. Phys. Lett.* **57** 2374
[23] Al Qaradawi I, Charlton M, Borozan I and Whitehead R 2000 *J. Phys. B: At. Mol. Opt. Phys.* **33** 2725
[24] Jørgensen L V *et al* (ATHENA collaboration) 2005 *Phys. Rev. Lett.* **95** 025002
[25] Funakoshi R *et al* (ATHENA collaboration) 2007 *Phys. Rev. A* **76** 012713
[26] Amoretti M *et al* (ATHENA collaboration) 2002 *Nature* **419** 456
[27] Madsen N *et al* (ATHENA collaboration) 2005 *Phys. Rev. Lett.* **94** 033403
[28] Andresen G B *et al* (ALPHA collaboration) 2010 in preparation
[29] Amoretti M *et al* (ATHENA collaboration) 2004 *Phys. Lett. B* **578** 23
[30] Gabrielse G *et al* (ATRAP collaboration) 2002 *Phys. Rev. Lett.* **89** 233401
[31] Robicheaux F 2004 *Phys. Rev. A* **70** 022510
[32] Robicheaux F and Hanson J D 2004 *Phys. Rev. A* **69** 010701
[33] Robicheaux F 2008 *J. Phys. B: At. Mol. Opt. Phys.* **41** 192001